

# Research Article





How to cite: Angew. Chem. Int. Ed. 2025, 64, e202417251 doi.org/10.1002/anie.202417251

# **Electrothermal Conversion of Methane to Methanol at Room Temperature with Phosphotungstic Acid**

Jinquan Chang, Sikai Wang, Max J. Hülsey, Sheng Zhang, Shi Nee Lou, Xinbin Ma,\* and Ning Yan\*

Abstract: Traditional methods for the aerobic oxidation of methane to methanol frequently require the use of noble metal catalysts or flammable H<sub>2</sub>-O<sub>2</sub> mixtures. While electrochemical methods enhance safety and may avoid the use of noble metals, these processes suffer from low yields due to limited current density and/or low selectivity. Here, we design an electrothermal process to conduct aerobic oxidation of methane to methanol at room temperature using phosphotungstic acid (PTA) as a redox mediator. When electrochemically reduced, PTA activates methane with O2 to produce methanol selectively. The optimum productivity reaches 29.45  $\mu mol\ g_{PTA}^{-1}h^{-1}$  with approximately 20.3% overall electron yield. Under continuous operation, we achieved 19.90  $\mu mol~g_{PTA}^{-1}h^{-1}$  catalytic activity, over 74.3% methanol selectivity, and 10 hours durability. This approach leverages reduced PTA to initiate thermal catalysis in solution phase, addressing slow methane oxidation kinetics and preventing overoxidations on electrode surfaces. The current density towards methanol production increased over 40 times compared with direct electrochemical processes. The in situ generated hydroxyl radical, from the reaction of reduced PTA and oxygen, plays an important role in the methane conversion. This study demonstrates reduced polyoxotungstate as a viable platform to integrate thermo- and electrochemical methane oxidation at ambient condi-

#### Introduction

Industrial production of methanol (CH<sub>3</sub>OH) from methane (CH<sub>4</sub>) relies on a two-step high temperature, high pressure process via syngas (Figure S1a).<sup>[1]</sup> In comparison, the direct one-step oxidation of CH<sub>4</sub> to CH<sub>3</sub>OH is difficult because of CH4's stable C-H bonds and CH3OH's susceptibility to overoxidation.<sup>[2]</sup> Chemical looping processes have been developed to oxidize CH4 to CH3OH, preventing direct contact between O2 and CH4 to reduce overoxidation, but these face issues like high heat requirements, coke deposition, and catalyst sintering. [2a,3] Researchers have also reported single-step CH<sub>4</sub> activation using metal species like Pt(II), Pd(II) and Pb(IV) in sulfuric acid/trifluoroacetic acid solvent<sup>[4]</sup> at temperatures of 80-220 °C (Figure S1b). Irrespective of the mechanistic details, these metal species activate the C-H bond of CH<sub>4</sub>, followed by reductive elimination that generates CH<sub>3</sub>OH and a lower valent metal species. This sequence requires the addition of chemical oxidants such as H<sub>2</sub>O<sub>2</sub>, O<sub>2</sub>, K<sub>2</sub>S<sub>2</sub>O<sub>8</sub>, or peroxytrifluoroacetic acid to reoxidize reduced metal species.  $^{[4b]}$  Moreover,  $H_2O_2$ is used to oxidize CH4 to oxygenates under mild and noncorrosive conditions at 50-180°C (Figure S1b).<sup>[5]</sup> To address the issue of overoxidation by excessive amount of H<sub>2</sub>O<sub>2</sub>, the in situ synthesis of H<sub>2</sub>O<sub>2</sub> from H<sub>2</sub>/O<sub>2</sub> mixtures, catalyzed by AuPd bimetallic nanoparticles, has been integrated into CH<sub>4</sub> oxidation processes. [6] Nonetheless, the cost of catalysts/ oxidants and the employment of hazardous chemicals have limited the utility of those process.

Recently, electrocatalytic conversion of CH<sub>4</sub> has been reported, bringing advantages like mild reaction condition and innovative reaction pathway.[7] Studies have demonstrated that CH<sub>4</sub> can be directly activated on the electro-

[\*] J. Chang, Dr. S. Wang, Prof. X. Ma, Prof. N. Yan Joint School of National University of Singapore and Tianjin International Campus of Tianiin University Binhai New City, Fuzhou 350207 (China)

J. Chang, Dr. S. Wang, Dr. M. J. Hülsey, Prof. N. Yan Department of Chemical and Biomolecular Engineering National University of Singapore

4 Engineering Drive 4, Singapore 117585 (Singapore) E-mail: ning.yan@nus.edu.sg

Prof. S. Zhang, Prof. X. Ma

Key Laboratory for Green Chemical Technology of Ministry of

Collaborative Innovation Center of Chemical Science and Engineer-

School of Chemical Engineering and Technology Tianjin University, Tianjin 300072 (China)

E-mail: xbma@tju.edu.cn

Prof. S. Zhang, Prof. X. Ma

Haihe Laboratory of Sustainable Chemical Transformations

Tianjin University, Tianjin 300192 (China)

Prof. S. Nee Lou

School of Chemical Engineering and Technology

Tianjin University, Tianjin 300072 (China)

5213773, 2025, 5, Downloaded from https://onlinelibrary.wiley.com/doi/10.1002/anie.202417251 by Dalian Institute Of Chemical, Wiley Online Library on [03/11/2025]. See the Terms and Conditions (https://onlinelibrary.wiley.com/rems-and-conditions) on Wiley Online Library for rules of use; OA articles are governed by the applicable Creative Commons. Licensen

catalyst surface such as NiO/Ni<sup>[8]</sup> and TiO<sub>2</sub>/RuO<sub>2</sub>/V<sub>2</sub>O<sub>52</sub><sup>[9]</sup> showing 13-97 % CH<sub>3</sub>OH selectivity (Table S1). However, the electrocatalysis was highly restricted by the low electrochemical surface area and gas transport of CH4 to the electrode surface (Figure S1c), resulting in very low current density ( $<40 \,\mu\text{A}\,\text{cm}^{-2}$ , with effective current density for CH<sub>3</sub>OH production less than 10 µA cm<sup>-2</sup>) and hard-to-avoid overoxidation by anodic potential.[10,11] Besides generating active oxygen species from H<sub>2</sub>O, CO<sub>3</sub><sup>2-</sup> was also developed as an oxygen donor on the anodic electrode surface. [12] ZrO<sub>2</sub>: NiCo<sub>2</sub>O<sub>4</sub>, NiO/ZnO, Fe<sub>2</sub>O<sub>3</sub> and CuO/CeO<sub>2</sub> were shown to produce O\* from CO<sub>3</sub><sup>2-</sup>, which then facilitated the breaking of C-H bonds in CH<sub>4</sub>. The activated CH<sub>3</sub>\* was subsequently electrochemically transformed into valuable products, including ethanol, propanol and propionic acid.[12b-f] The isotope labeling experiment confirmed that the carbon and oxygen in these products originate from CH<sub>4</sub> and CO<sub>3</sub><sup>2-</sup>, respectively.[12c-f]

The combination of electro- and thermo- catalysis has led to an indirect electrochemical CH4 activation process.<sup>[7a,13]</sup> As shown in Figure S1d, applying potentials upward of 1.6-2.2 V versus Hg<sub>2</sub>SO<sub>4</sub>/Hg produces high-valent metal cations at the anode, which react with CH<sub>4</sub> and H<sub>2</sub>SO<sub>4</sub> to produce methyl bisulfate. This method eliminates the use of hazardous oxidants and is more controllable. [4d,14] Similarly, electrochemical processes have been tested with trifluoroacetic acid solvent, Pd(IV) trifluoroacetate oxidant, and potassium trifluoroacetate electrolyte. While versatile for various gaseous alkanes, its Faradaic efficiency (FE) for CH<sub>4</sub> was just about 2 %.<sup>[15]</sup>

Furthermore, cathodic aerobic activation employing in situ generated H<sub>2</sub>O<sub>2</sub> from a two-electron oxygen reduction reaction was introduced. Due to the low solubility of CH<sub>4</sub> in water and the low selectivity of reactive oxygen species (ROS, as detailed in Eq. 1-3), the total electron yield towards organooxygen compounds rarely surpassed 12%. The primary oxygenates' selectivity, including CH<sub>3</sub>OH and CH<sub>3</sub>OOH, remained under 20% for cathodic methane conversion. [16] Electrochemical imitation of CH<sub>4</sub> monooxygenase (MMO) process<sup>[17]</sup> was also developed using solution phase with iron-tungsten oxide as electrolyte, from which light hydrocarbons were aerobically oxidized to various

oxygenates in electrolyte near the cathode following an inner sphere electron transfer mechanism. [18] Nonetheless, the oxidation of CH<sub>4</sub> was sluggish with a FE of around 0.7 % and no CH<sub>3</sub>OH or CH<sub>3</sub>OOH was detected in the final products. In light of these earlier findings, developing a strategy for the direct and selective generation of CH<sub>3</sub>OH from CH<sub>4</sub> without using corrosive acid, H<sub>2</sub> and noble metals is highly demanded.[18b]

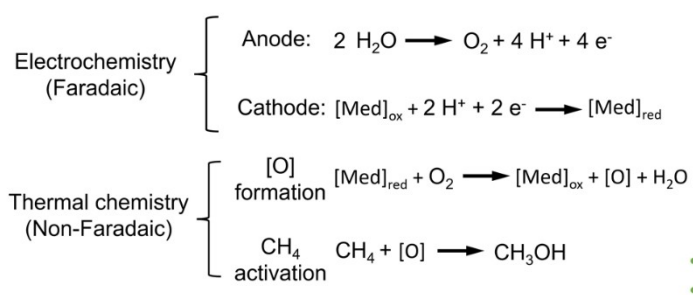
Cathodic O<sub>2</sub> activation : 
$$O_2 + 2 H^+ + 2 e^- \rightarrow H_2O_2$$
 (1)

ROS generation : 
$$H_2O_2 \rightarrow 2 \ HO^{\bullet}$$
 or 
$$H_2O_2 + H^+ + e^- \rightarrow HO^{\bullet} + H_2O$$
 (2)

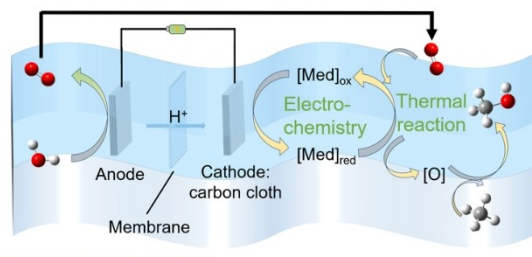
Chemical CH<sub>4</sub> activation : 
$$CH_4 + {}^{\bullet}OH \rightarrow CH_3 + H_2O$$
 (3)

Polyoxometalates (POMs), such as phosphomolybdic (PMA) and phosphotungstic acid (PTA), have been utilized as catalysts in various reactions due to their acidity and redox properties.<sup>[19]</sup> CH<sub>4</sub> can be activated by POM-based catalysts in conjunction with noble metals.<sup>[20]</sup> For instance, Pd supported on PMA offered considerable activity for CH<sub>4</sub> to CH<sub>3</sub>OH in the presence of a H<sub>2</sub>-O<sub>2</sub> mixture. [21] A disadvantage of the work, however, is the use of noble metal Pd and the requirements of H<sub>2</sub> as co-feed. Built upon our earlier work on the facile electron transfer between electrode and POMs,<sup>[22]</sup>

here, we intend to design an electrothermal process (Scheme 1) to convert CH<sub>4</sub> into primary oxygenates (CH<sub>3</sub>OH and CH<sub>3</sub>OOH, or combined as CH<sub>3</sub>O<sub>x</sub>H with x =1,2) at room temperature under aerobic conditions without the use of noble metals and H2. Since CH3OOH can be converted to CH<sub>3</sub>OH easily (see details in Conversion of CH<sub>3</sub>OOH to CH<sub>3</sub>OH in Supporting Information, Figure S2), we considered CH<sub>3</sub>OOH as a(an) variant/intermediate of CH<sub>3</sub>OH. Specifically, we employ the cathodic potential to reduce the POMs. Then O2 and subsequently CH4 was activated by reduced POM to CH<sub>3</sub>O<sub>x</sub>H with up to 100% selectivity and 20.3 % electron yield (EY, refer to Supporting Information for definitions). PTA was chosen as a model compound for study due to its redox reversibility and its stability.



Total:  $CH_4 + 6 H^+ + 6 e^- + 2O_2 \longrightarrow CH_3OH + 3 H_2O$ 



- Room temperature
- Noble metal & H<sub>2</sub> & highly corrosive acid free system
- High CH<sub>3</sub>OH productivity and selectivity
- · Mild applied potential (avoid overreaction)

Scheme 1. Proposed strategy for electrothermal CH<sub>4</sub> activation to CH<sub>3</sub>OH via several redox cycles.



#### Results and Discussion

The electrochemical properties of PTA were investigated by a cyclic voltammetry (CV) curve as shown in Figure S3a, with the half wave potential  $(E_{1/2})$  of first and second electron transfer occurring at -33.5 and -310 mV versus Ag/AgCl (approximately 268.5 and -8 mV versus RHE, the pH ~1.84 for 5 mM PTA solution (Figure S4)), respectively, consistent with previous reports. [23] The subsequent reduction of PTA, while in principle possible (green rectangular marker in Figure S3a), is limited by the electrochemical stability of water and convoluted by concomitant hydrogen evolution even on relatively poor HER catalysts like carbon<sup>[24]</sup> and was thus not further considered in our study. One-/two-electron reduced PTA (PTA<sub>1e</sub> and PTA<sub>2e</sub>) was readily obtained from chronoamperometry at constant negative potential within 15 min under inert atmosphere in a divided electrochemical cell (Figures 1a and S3b-d) using a carbon cloth electrode. Hydrogen evolution was suppressed and the color of the electrolyte changed from colorless to dark blue due to the formation of reduced PTA - so called "heteropoly blues" (Figure S3d). [25] The efficiency of electroreduction was analyzed by the total number of electrons

transferred into PTA molecules via X-ray photoelectron spectroscopy (XPS) (Figure 1b). The XPS samples were obtained from freeze dryer, stored in glove box, and transferred into XPS instrument using a vacuum transfer module (see details in Characterization). A new symmetric pair of peaks located at 37.0 and 34.9 eV appeared for the PTA<sub>red</sub> sample corresponding to  $W^{(V)}$   $4f_{5/2}$  and  $W^{(V)}$   $4f_{7/2}$ , respectively. [26] The  $W^{(V)}$  proportions for  $PTA_{1e}$  and  $PTA_{2e}$ were 9.0% and 17.7%, aligning with estimates for one and two electron-reduction scenarios, respectively. We did not observe the formation of  $W^{(\text{IV})}$  species, suggesting the composition of PTA is  $[PW^{(\mathrm{VI})}{}_{10}\hat{W^{(\mathrm{V})}}{}_{2}O_{40}]^{5-}$  in the twoelectron reduced state. The structure of PTA remained intact after reduction, inferred from the virtually identical X-ray diffraction (XRD) patterns and Fourier transform infrared (FTIR) spectra (Figures S5a, S5b). Concurrently, the most abundant mass-to-charge ratio (m/z) of PTA<sub>red</sub> locates at 1439.1, 1439.6 and 1440.1, respectively, for original PTA (PTA<sub>ox</sub>), PTA<sub>1e</sub> and PTA<sub>2e</sub> (the additional charges are countered by protons from solution (Figure S4)), as revealed by electrospray ionization mass spectrometry (ESI-MS, Figure 1c). These confirmed the facile electrochemical

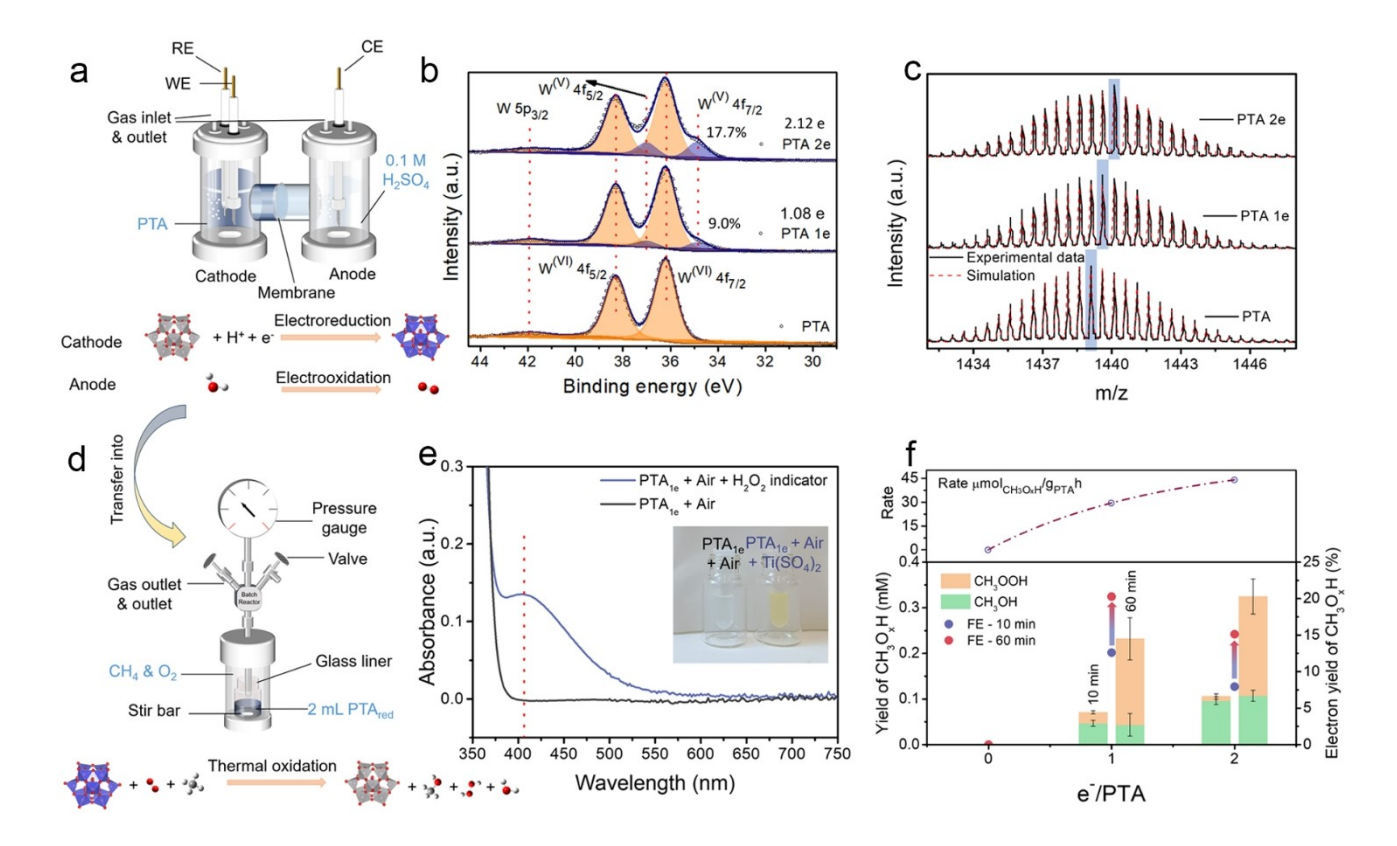


Figure 1. Electrochemically reduced phosphotungstic acid (PTA<sub>red</sub>) and its reaction with air and CH<sub>4</sub>. a, d) The illustration of electroreduction process and thermal reaction procedure. RE, CE and WE represent reference, counter and working electrode, respectively. b, c) X-ray photoelectron spectroscopy (XPS) and electrospray ionization mass spectrometry (ESI-MS) of original PTA, one-/two- electron reduced PTA (PTA<sub>1e</sub> and PTA<sub>2e</sub>), respectively. e) ultraviolet-visible spectrum (UV/Vis) of solution (after reoxidation) with titanium (IV) sulfate (H<sub>2</sub>O<sub>2</sub> indicator), and f) the reaction performance of original 5 mM PTA, PTA<sub>1e</sub> and PTA<sub>2e</sub> under 60 bar of CH<sub>4</sub> and 1 bar of air. Typically, 2 mL of a 5 mM PTA<sub>red</sub> solution was stored in a batch reactor (33 mL gas volume, as illustrated in d), stirred at 800 rpm at room temperature for reaction time of 10 and 60 min. The average values reported here are repeated three times. EY represents electron yield.

reduction of PTA on carbon electrodes and the structural stability of reduced PTA in aqueous solutions.

Following electroreduction, 2 mL of the deep blue PTA solution was moved to a batch reactor with a stirrer and subjected to 60 bar of CH<sub>4</sub> and 1 bar of air (Figure 1d). After reaction, the liquid phase was analyzed by ultravioletvisible spectroscopy (UV/Vis) (Figures 1e, S6 and S7) and <sup>1</sup>H nuclear magnetic resonance (NMR) spectroscopy (typical <sup>1</sup>H NMR spectra are shown in Figures S8–S10, using CH<sub>3</sub>CN as the interior standard and calibration curves are shown in Figure S11), while the gas phase was characterized by gas chromatograph (GC) coupled to a methanizer and a flame ionization detector (see details in Characterization). Importantly, we observed the formation of CH<sub>3</sub>OH and CH<sub>3</sub>OOH, demonstrating the feasibility of aerobic CH<sub>4</sub> oxidation by PTA<sub>red</sub> (Figure 1f). Reaction rates of PTA<sub>1e</sub> and PTA<sub>2e</sub> system, determined by the yield after 10 min of reaction (broadly in line with the average values, as outline in Supplementary Note I and Figure S12), were 29.5 and 44.0  $\mu mol_{CH3OxH}g_{PTA}^{-1}h^{-1}$ , respectively, comparable to other catalytic systems in previous reports (Table S1). The electron yield towards CH3OxH in the one-electron reduced PTA system was relatively high, at 12.61 % initially and 20.27 % towards the end. In contrast, a 30-40 % drop was noted under the PTA<sub>2e</sub> condition which is due to the PTA<sub>2e</sub> promoted the overreduction of O<sub>2</sub> to H<sub>2</sub>O. Reasons such as the higher reducing ability (Figures S13a, S13b), the pH effect (Figures S4 and S13c) and reaction kinetics may account for the observed overreduction by PTA<sub>2e</sub> (details can be found in supplementary Note II). Thus, maintaining the 1e reduction state of PTA during electroreduction is preferable. No carbon-based products were detected using non-reduced PTA (PTAox), highlighting the importance of PTA's reduction state for methane oxidation.

After the reaction, the solution changed back to colorless suggesting reoxidation of PTA (Figure 1e). Meanwhile, the structure simultaneously reverted to PTA $_{ox}$  (Figure S5c). However, reacting with CH $_{4}$  alone does not lead to color change. Adding titanium (IV) sulfate to the PTA $_{red}$  solution in the presence of air, the color changed to yellow. These suggest that electrons were transferred from PTA $_{red}$  to oxygen resulting in the formation of H $_{2}$ O $_{2}$  (as shown in Table S1) and H $_{2}$ O, $^{[27]}$  following an outer-sphere mechanism which has been demonstrated by stopped-flow techniques and Marcus theory. $^{[28]}$ 

Rates of reoxidation of PTA<sub>red</sub> in the presence of  $O_2$  were determined by UV/Vis spectroscopy. The intensity decrease of the peaks at 750 and 495 nm—attributed to metal-to-metal intervalence charge transfer (IVCT) and d-d transition band, respectively (Figure S14),<sup>[29]</sup>-were measured over time at different  $O_2$  partial pressures. We observed a pseudo first order relationship between PTA<sub>red</sub> reoxidation and the concentrations of PTA and  $O_2$  (Figures S15 and S16). The CH<sub>3</sub>O<sub>x</sub>H generation rates increased 4.2 folds when  $O_2$  partial pressure increased from 50 mbar to 1 bar, peaking at  $72.5 \, \mu mol_{CH3OxH}g_{PTA}^{-1}h^{-1}$  at 1 bar  $O_2$ . No other carbon-containing products were detected at  $O_2$  pressures below 0.2 bar. However, formaldehyde (HCHO), an overoxidation product, appeared after 30 min reaction at 1 bar

O<sub>2</sub> (Figure S17). Despite this, the final yields of CH<sub>3</sub>O<sub>x</sub>H (approximately 0.25 mM) and H<sub>2</sub>O<sub>2</sub> (approximately 0.7 mM) remained unchanged (Figures 2a and b). On the other hand, the product selectivity changed from H<sub>2</sub>O<sub>2</sub> to CH<sub>3</sub>O<sub>x</sub>H when reaction progresses. More specifically, the electron yield of CH<sub>3</sub>O<sub>x</sub>H and FE of H<sub>2</sub>O<sub>2</sub> changed from 14.3 % and 39.8 % to 21.7% and 26.4% for initial and final reaction stage, respectively, suggesting that H<sub>2</sub>O<sub>2</sub> generation and CH<sub>4</sub> activation may be consecutive steps. The concentration of PTA<sub>red</sub> influenced the electron transfer rate from PTA<sub>red</sub> to O<sub>2</sub>, affecting the FE of H<sub>2</sub>O<sub>2</sub> (from 34.3 % to 4.9 %), but having little effect on the electron yield of CH<sub>3</sub>O<sub>x</sub>H (approximately 20%, Figures 2c and d). As a consequence, the reaction kinetics towards CH<sub>3</sub>O<sub>x</sub>H production normalized by the amount of PTA remained unchanged during the reaction. These results indicated the existence of competitive reactions like H<sub>2</sub>O<sub>2</sub> decomposition, corresponding to the observation of a slight acceleration of the oxidation rate of PTA<sub>red</sub> at higher concentrations (Figure S18b, and magenta and orange fitting curves in Figure S16c). Over a

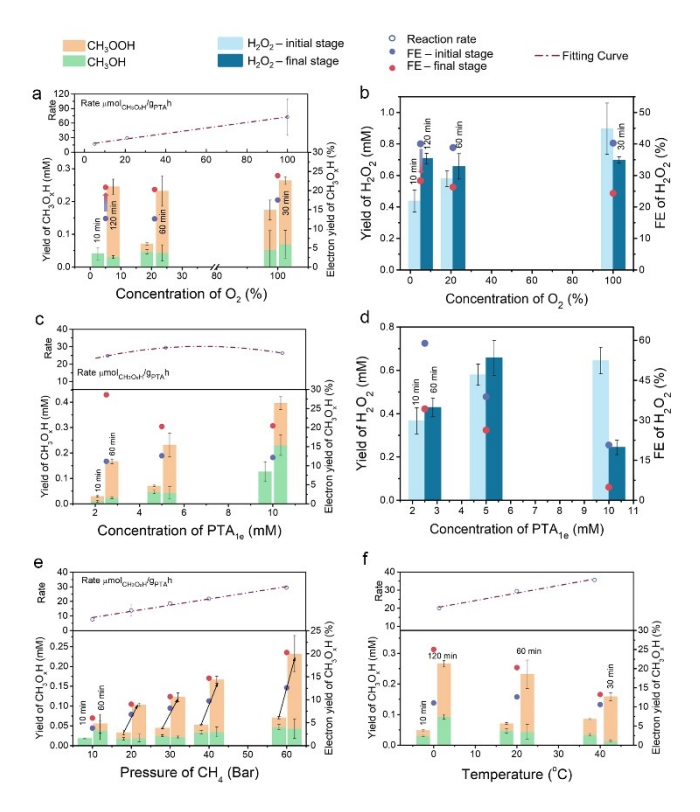


**Figure 2.** CH<sub>4</sub> activation by reduced PTA (PTA<sub>red</sub>) and air in batch reactor. The influence of a, b) concentration of  $O_2$ , c, d) PTA<sub>red</sub>, e) pressure of CH<sub>4</sub> and f) temperature on the reaction kinetics, yield and selectivity towards methyl derivates (CH<sub>3</sub>O<sub>x</sub>H) and H<sub>2</sub>O<sub>2</sub> for the initial (10 min) and final reaction stage (typically 60 min, but 120 min and 30 min for 50 mbar and 1 bar  $O_2$  or 0°C and 40°C experiment, respectively). The typical reaction conditions were 60 bar of CH<sub>4</sub>, 1 bar of air, and 2 mL of a 5 mM PTA<sub>1e</sub> solution in a batch reactor (33 mL), stirred at 800 rpm at room temperature for reaction time of 10 and 60 min. All reported data collected from at least three independent trials, and the average values are reported here. EY represents electron yield, analogous to Faradaic efficiency (FE) in the context of faradaic processes (H<sub>2</sub>O<sub>2</sub> production).

wide range of 10–60 bar  $CH_4$  pressures, the reaction followed a pseudo-first-order kinetics (Figure 2e). This is consistent with previous reports ascribing this trend to  $CH_4$  activation being a rate-determining step. [14b] The rate of electron transfer from  $PTA_{\rm red}$  and the yield of  $H_2O_2$  remained largely invariant with  $CH_4$  pressure (Figures S18c and S18d), demonstrating that  $CH_4$  does not affect dioxygen activation.

When reaction temperature increased, the  $CH_3O_xH$  production rate (calculated from 10 min reaction, Figure 2f), electron transfer rate (Figure S18e) and  $H_2O_2$  productivity

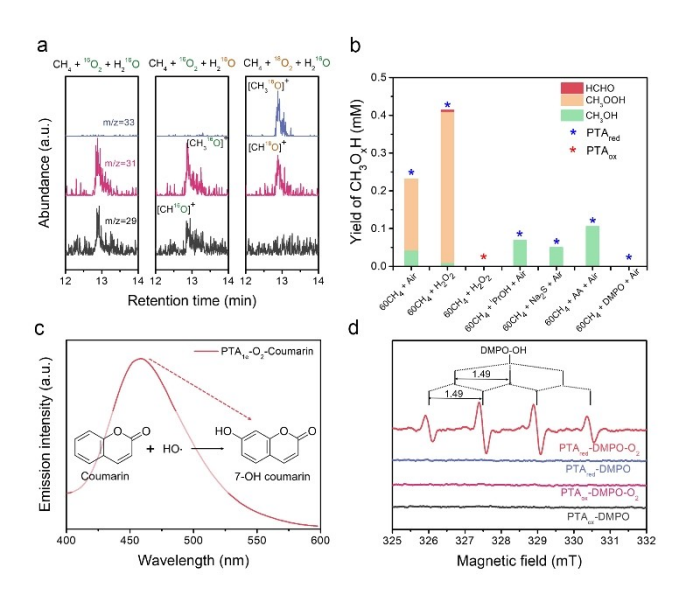


Figure 3. Mechanism understanding of CH<sub>4</sub> partial oxidation by PTA<sub>red</sub> and air. Control experiments under a) different isotope-labelled reactants, b) different reaction conditions. c) Fluorescence spectra of coumarin with PTA<sub>red</sub> and air, d) electron paramagnetic resonance (EPR) spectra of PTA<sub>ox</sub> (black), PTA<sub>red</sub> (blue), PTA<sub>ox</sub>/air (pink) and PTA<sub>red</sub>/air (red) system.

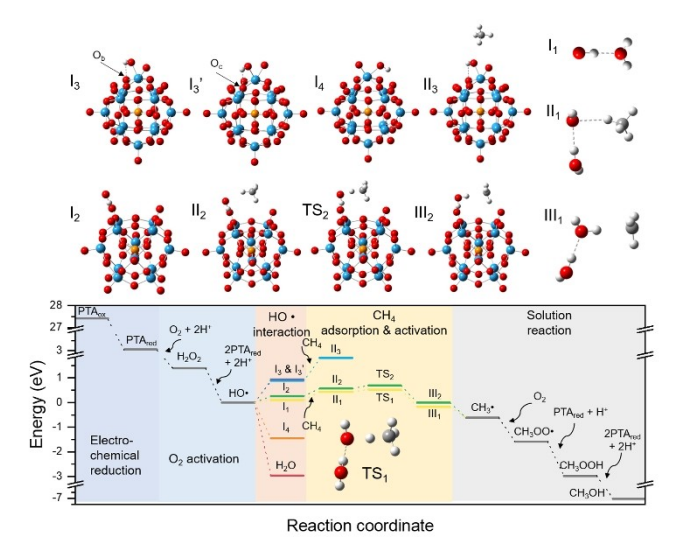
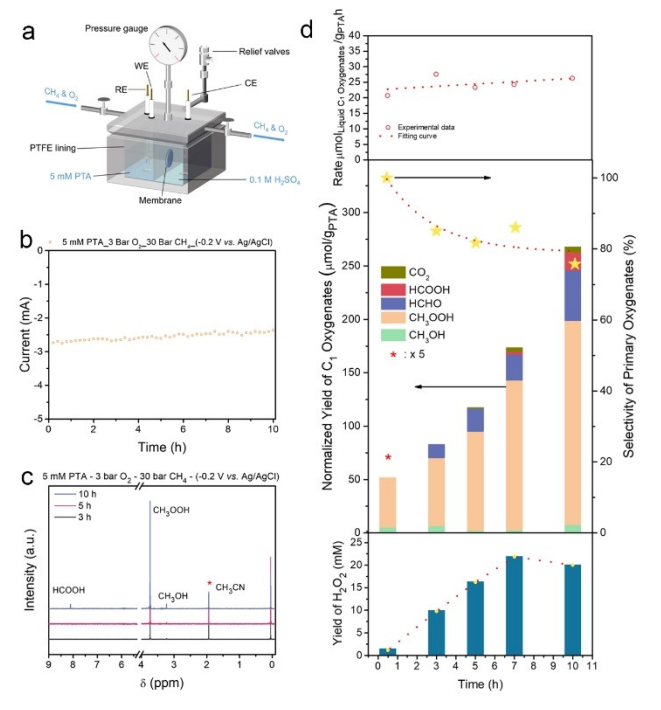


Figure 4. Illustration of structure intermediates and related energy

(Figure S18f) increased at the expense of  $CH_3O_xH$  selectivity (as observed at the end of the reaction). This could be explained by lower  $CH_4$  solubility or the acceleration of 2-electon  $O_2$  reduction accompanied by lower ROS generation efficiency at higher temperatures. As such, electron yields increased to around 25 % when the reaction was conducted at 0°C. Notably, the ratio between  $CH_3OH$  and  $CH_3OOH$  increased with higher concentration of  $PTA_{red}$  but decreased with temperature, a fact that will be discussed in more detail in a later section. No significant oxidation of  $CH_3OH$  was observed in this two-step reaction process (Figure S19), which may be attributed to the lower concentration of  $CH_3OH$  and the protective effect of  $PTA_{red}$ .

We propose that the partial oxidation of  $CH_4$  by  $PTA_{red}$  and  $O_2$  follows a three-step process, including oxygen activation, ROS production, and  $CH_4$  activation. We first investigated the oxygen source for the reaction by isotope labelling experiments using  $^{18}O_2$  and  $H_2^{18}O$  (Figure 3a). Two major peaks at  $m/z\!=\!31$  and  $m/z\!=\!29$  representative  $[CH_3^{16}O]^+$  and  $[CH^{16}O]^+$  (the fragments of  $CH_3^{16}OH$  and  $HCH^{16}O$ , the overoxidation product under prolonged operation, Figure 5d)), were formed in the presence of  $^{16}O_2$ , regardless of whether  $H_2^{16}O$  or  $H_2^{18}O$  was used. In contrast, the two peaks shift to  $m/z\!=\!33$  and  $m/z\!=\!31$ , respectively,



**Figure 5.** Continuous operation of electrothermal process for CH<sub>4</sub> partial oxidation. a) Scheme illustration of high-pressure H-type electrolytic cell, b) durability test of the electrothermal process under 30 bar CH<sub>4</sub>, 3 bar O<sub>2</sub> at -0.2 V versus Ag/AgCl, c) the  $^{1}$ H nuclear magnetic resonance (NMR) spectrum with distinct reaction time and d) electrothermal kinetics and products analysis. The typical reaction conditions were 30 bar of CH<sub>4</sub>, 3 bar of O<sub>2</sub>, and 10 mL of a 5 mM PTA<sub>ox</sub> electrolyte (cathodic compartment) in a high-pressure electrochemical cell (-100 mL), stirred at 1200 rpm under room temperature with a potential of -0.2 V versus Ag/AgCl.

when using <sup>18</sup>O<sub>2</sub>, indicating the formation of <sup>18</sup>O-labelled methanol (CH<sub>3</sub><sup>18</sup>OH) and formaldehyde (HCH<sup>18</sup>O), proving that oxygen in organic compound comes exclusively from O<sub>2</sub>. Then, experiments using H<sub>2</sub>O<sub>2</sub> rather than O<sub>2</sub> as terminal oxidant were conducted with PTA<sub>red</sub> or PTA<sub>ox</sub>. While catalytic performance comparable to that in the presence of O<sub>2</sub> was observed for PTA<sub>red</sub>, PTA<sub>ox</sub> still did not yield any CH<sub>3</sub>O<sub>x</sub>H products in the presence of H<sub>2</sub>O<sub>2</sub> (Figure 3b). This sharp contrast demonstrates the significance of employing reduced PTA even beyond the formation of H<sub>2</sub>O<sub>2</sub> from O<sub>2</sub>.

To uncover the active species, a fluorescein-based probe molecule like coumarin was employed to detect the potential HO<sup>o</sup> in the solution. A peak located at 455 nm was observed after the reaction with electrolyte containing PTA<sub>red</sub> and O<sub>2</sub>, indicating the formation of 7-OH coumarin (Figure 3c).<sup>[30]</sup> Concurrently, the electron paramagnetic resonance (EPR) experiments using 5,5-dimethyl-1-pyrroline Noxide (DMPO) radical trapping agent were implemented. In contrast to the EPR-silent PTAox system and our previous Mo-based polyoxometalate catalyst, the appearance of characteristic quadruple peaks (1:2:2:1) for trapped HO radicals in  $PTA_{red}/O_2$  system clearly indicated the production of such species during the reaction (Figure 3d).[31] To mitigate the interference from superoxide anions/hydroperoxyl radicals (O<sub>2</sub>•-/HOO•) in HO• detection, dimethyl sulfoxide (DMSO)[32] was introduced during the EPR testing (refer to Supplementary Note III for details). The absence of DMPO signals (Figure S20) confirms the production of  $HO^{\bullet}$  in  $PTA_{red}/O_2$  system. While  $O_2^{\bullet-}/HOO^{\bullet}$  radicals<sup>[28]</sup> are significant intermediates in O2 reduction, they are not readily detectable due to kinetic limitations (Supplementary Note III). Thus, the focus remains on the role of HO. radicals in the reaction. Subsequently, experiments of CH<sub>4</sub> oxidation were conducted in the presence of HO radical scavengers, such as iso-propanol (iPrOH), sodium sulfide (Na<sub>2</sub>S), ascorbic acid (AA) and DMPO. The yield of CH<sub>3</sub>OOH dropped in the presence of all four inhibitors (Figure 3b), strengthening the active role of HO• in CH<sub>4</sub> activation.[16,33] The formation of CH<sub>3</sub>OH, however, remained constant in the presence of Na<sub>2</sub>S or even increased for <sup>i</sup>PrOH and AA, respectively (Figure 3b). The increase in CH<sub>3</sub>OH could be related to changes in the lifetime of PTA<sub>red</sub> (Figure S21) analogous to what we found for catalysis with PMA. [21] The generated PTA<sub>red</sub> promoted the formation of HO radicals in solution, counteracting the consumption effects of the sacrificial reaction. Additionally, the increased or maintained PTA<sub>red</sub> concentration facilitated the conversion of CH<sub>3</sub>OOH to CH<sub>3</sub>OH (Figure S2), aligning with the observed effects of PTA<sub>red</sub> as well as temperature on reaction performance. Notably, the use of DMPO as a scavenger completely suppressed the oxidation of CH<sub>4</sub>, highlighting the significant role of HO<sup>•</sup> in this process.<sup>[20a]</sup> The possibility of reactions occurring on the surface of PTA was also considered. Since electron transfer between O<sub>2</sub>/ H<sub>2</sub>O<sub>2</sub> and PTA<sub>red</sub> occurs through an outer-sphere mechanism,  $^{[28,34]}$  and no reaction was observed in the  $\mathrm{O}_2/$ H<sub>2</sub>O<sub>2</sub> and PTA<sub>ox</sub> system, we explored the potential for CH<sub>4</sub> As shown in Figure 4,  $PTA_{red}$  is electrochemically produced from  $PTA_{ox}$ , with an absolute Gibbs free energy change ( $\Delta G$ ) of -4.059 eV (192.2 mV versus RHE, Supplementary Note IV), consistent with the results shown in Figure S3a.  $PTA_{red}$  then acts as the active species, facilitating the generation of  $HO^{\bullet}$  through a 3-electron  $O_2$  reduction reaction. Three interaction scenarios involving  $HO^{\bullet}$  radicals are explored: 1) hydrogen bonding with  $H_2O$  or  $PTA_{ox}$  (Structures  $I_1$  and  $I_2$ , respectively); 2) W–O bonding with  $PTA_{ox}$  (Structures  $I_3$  and  $I_3$ ) or  $PTA_{red}$  (Structure  $I_4$ ); and 3) electron transfer from  $PTA_{red}$ , leading to overreduction and the formation of  $H_2O$ .

The formation of Structures  $I_3$  and  $I_3{'}$  results in increases in enthalpy ( $\Delta H$ , Figure S22) and  $\Delta G$  (Figure 4) of 0.47/0.52 eV and 0.85/0.90 eV, respectively, indicating that W–O bond formation between HO $^{\bullet}$  radicals and PTA $_{ox}$  is energetically unfavorable. While W–O bond formation with PTA $_{red}$  is energetically possible, it is less advantageous compared to the overreduction process. Additionally, formation of Structure  $I_4$  causes a change in spin multiplicity (from doublet to singlet), complicating subsequent C–H activation. Consequently, capturing free radicals through structural changes in the PTA $_{ox/red}$  cluster is considered less effective. Therefore, we believe that the reaction predominantly proceeds via the solution pathway.

HO has been reported to be active in the solution phase abstraction of H atoms from CH<sub>4</sub> to form CH<sub>3</sub>\* (positive order in CH<sub>4</sub>).<sup>[35]</sup> Two viable scenarios involving hydrogen bonding between radicals and H<sub>2</sub>O<sup>[36]</sup> or PTA<sub>ox</sub> are proposed. The relatively small free energy barriers (0.53 eV for TS<sub>1</sub> and 0.69 eV for TS<sub>2</sub>) indicate that the H abstraction reaction is feasible at room temperature.<sup>[37]</sup> Methyl radicals (CH3°) produced in the reaction rapidly combines with dissolved O<sub>2</sub> to form CH<sub>3</sub>OOH. [6b,38] CH<sub>3</sub>OOH then reacts with PTA<sub>red</sub> and protons in the solution to produce CH<sub>3</sub>OH. Direct termination of CH3 by HOO or HO is also considered, but due to the high reactivity and low concentration of radicals, such collisions are highly unlikely (Figures S23-S25, Supplementary Note IV), rendering these pathways kinetically infeasible. Nevertheless, increasing the pressure of CH<sub>4</sub>, as well as the concentrations of HO<sup>•</sup> and PTA<sub>red</sub>, will enhance the production of CH<sub>3</sub>OH.

Our discovery that mildly reduced PTA can convert  $\mathrm{CH_4}$  to methanol at room temperature in an aerobic environment led us to develop an electrothermal process that combines PTA electroreduction with  $\mathrm{CH_4}$  thermal oxidation. Due to the low solubility of  $\mathrm{CH_4}$  in aqueous electrolytes, we employed a commercially available high-pressure electrochemical cell with compartments separated by a proton exchange membrane (Nafion-117) (Figure 4a). A carbon cloth or glassy carbon was used as working electrode (see details in Supporting Information) and experiments were run on potentostatically. Parameters such as  $\mathrm{O_2}$  pressure, PTA concentration and applied potential were optimized using this electrochemical cell (Figures S26–29). The products were analyzed by UV/Vis, NMR and GC after a certain amount of charge was passed between the two electrodes





(consistent with the amount of achieving  $PTA_{1e}$  state). No  $H_2$  was detected in any experiment. The system's reaction kinetics and PTA's reduction degree were revealed by the current value and open circuit potential (OCP, see details in Supporting Information, Figure S30), respectively.

The relatively stable currents for various O<sub>2</sub> pressures (except for 1 bar) and PTA concentrations (2.5-10 mM) at −0.2 V versus Ag/AgCl (approximately 0.1 V versus RHE) suggested the establishment of a rapid reaction equilibrium between electroreduction of PTA and thermal oxidation of PTA<sub>red</sub> by O<sub>2</sub> (Figures S26a and S27a). The decay of current value for 1 bar O<sub>2</sub> condition indicated the reaction kinetics was partially restricted by the reoxidation rate of PTA<sub>red</sub>, consistent with a higher reduction degree (around 0.85, Figure S30b) at the reaction equilibrium state. However, the relatively close current values (Figure S26a) for distinct O<sub>2</sub> pressures implied that O2 was saturated inside the reactor when the pressure was higher than 1 bar. As the O<sub>2</sub> pressure increased, the yield of H<sub>2</sub>O<sub>2</sub> rose dramatically, while the selectivity for CH<sub>3</sub>O<sub>2</sub>H first increased and then decreased (due to transformation to HCHO, Figures S26b-S26c). This observation demonstrates that while increased O<sub>2</sub> pressure promotes the formation of H<sub>2</sub>O<sub>2</sub>, it also accelerates the overoxidation of CH<sub>3</sub>O<sub>x</sub>H. The differing effect of O<sub>2</sub> pressure in high-pressure electrochemical cell versus batch reactor may stem from diffusion limitations, with the smaller batch reactor exhibiting more pronounced localized pressure effects due to its higher diffusion rates. The highest electron yield was achieved at ~12.5 % with a reaction rate of 21.20  $\mu mol_{CH3OxH}g_{PTA}^{-1}h^{-1}$  at 3 bar O<sub>2</sub> (Figures S26c, d). In contrast, the changes in current values for different PTA concentrations (Figure S27a) may be related to a higher concentration of PTA species near the electrode surface and O<sub>2</sub>, enhancing the electron shuttle effect between the electrode and the reactant (O<sub>2</sub>). Meanwhile, relatively linear relationships between the current value and PTA concentration were observed, supporting our previously detected firstorder kinetics. The concentration of PTA had little effect on the selectivity and reaction rate of CH<sub>3</sub>O<sub>2</sub>H but it did reduce the selectivity of H<sub>2</sub>O<sub>2</sub> (Figures S27b-d), aligning with the findings for the non-continuous process.

We also studied the effect of applied potential (Figures S28-S29). The current value increased with the negative potential indicating that the oxygen activation was limited by the rate of electron transfer from the electrode to PTA<sub>ox</sub>. Compared with the one-electron reduced experiment, a onehour experiment with different charge transfer number at various applied potentials (Figure S29) showed an increase in CH<sub>3</sub>O<sub>x</sub>H generation rate (Figures S28d and S29d) which could be related to a faster accumulation of ROS with reaction duration, suggesting a certain amount of ROS should be maintained to promote the activation of CH<sub>4</sub>, despite a high chance of overoxidation (Figure S34). The highest reaction rate reached 10.71  $\mu mol_{CH3OxH}h^{-1}$ , equivalent to 572.9  $\mu A cm^{-2}$  (1.0 cm<sup>-2</sup> electrode geometry), almost 40-fold current density enhancement compared to direct electrochemical processes (Table S1). Surprisingly, the electron yield was increased dramatically to 36.6 % at 0 V versus Ag/AgCl, consistent with the observation in separated process that milder reduction degree is more selective to oxidized methane species (Figure S30e) although the reaction kinetics was limited.

Next, -0.2 V (versus Ag/AgCl) was employed to test the system durability. The electrothermal CH<sub>4</sub> partial oxidation system was operated continuously for more than 10 h without obvious deactivation (Figure 4b). The main organic product was CH<sub>3</sub>OOH under the optimum working condition (Figure 4c) and the generation rate of primary oxygenates (CH<sub>3</sub>O<sub>x</sub>H) was as high as 19.90  $\mu mol_{CH3OxH}g_{PTA}^{-1}h^{-1}$ with 12.3 % electron yield and over 74.3 % selectivity (Figure 4d). Overoxidation products, HCHO and HCOOH, were detected after 1 h (Figure S31) and 7 h reaction, respectively. The concentration of H<sub>2</sub>O<sub>2</sub> accumulated to around 20 mM after 10 h reaction which could potentially be utilized by design of new redox cycle like Fe<sup>2+</sup>/Fe<sup>3+</sup> (Figure S32). However, the direct addition of 50 µM of Fe<sup>2+</sup>, Cu<sup>2+</sup>, or Mn<sup>2+</sup> to the solution resulted in a change of selectivity (Figures S32 and S33). Thus, a more designable strategy should be developed to maintain the selectivity and increase the reaction rate. Compared with pure H<sub>2</sub>SO<sub>4</sub> electrolyte system which mainly generates H<sub>2</sub>O<sub>2</sub> from traditional 2e-ORR process through carbon electrode, the current and yield of C<sub>1</sub> oxygenates of PTA electrolyte system has a dramatic increase (Figure S34). Thus, high electron yield, selectivity towards primary oxygenates and acceptable durability for CH<sub>4</sub> partial oxidation under mild reaction condition were successfully achieved without using noble metals and highly corrosive acids. The applied potential limits both CH<sub>3</sub>OH electroxidation and HER, as the electrode of carbon cloth is rather inert in the CH<sub>3</sub>OH electrooxidation and H2 evolution compared with noblemetal based electrocatalysts, as shown in Figure S35.

This electrothermal catalysis process exhibits notable scalability advantages over thermal, electrochemical and photocatalytic processes (Supplementary Note V and Table S3). The reaction rate can be enhanced up to 10 times by adjusting PTA concentration, O2 pressure and applied potential (Figure S36), though this may come at the cost of selectivity. Operating under mild conditions, this method reduces hazards associated with corrosive strong acid, and avoids the use of expensive or toxic materials (e.g., H<sub>2</sub>O<sub>2</sub>, transition metal cations). It also integrates well with renewable energy sources, offering both flexibility and sustainability. Additionally, this method is compatible with existing industrial electrolyzer infrastructure, facilitating a smoother transition to full-scale production. Nonetheless, challenges such as product separation, low conversion, and overoxidation (Figure S37) need to be addressed before large-scale implementation.

#### Conclusion

In summary, we report an electrothermal process for the aerobic oxidation of methane to methanol by reduced phosphotungstic acid at room temperature. Under the optimum conditions the system possesses a primary oxygenates productivity of 29.45 or 19.90  $\mu mol_{CH3OxH}g_{PTA}^{-1}h^{-1}$ ,





electron yields of 20.3 % and 12.3 % and almost 100 % and 74.3% selectivity for separate and continuous operation, respectively. The applied potential does not coincide with other reaction potentials such as methanol electrooxidation and hydrogen evolution, minimizing the notorious overreaction in methane conversion. The electrochemical and thermochemical reaction steps occur separately and are coupled through PTA as redox mediator. This setup allows for the conversion of intermittent renewable energy with readily obtainable oxidants like air or pure oxygen. In addition, the system is free from the utilization of noble metals, hazardous combustible reaction mixtures and corrosive acids, and operates at ambient temperature. From a mechanistic perspective, the selective oxidation of CH<sub>4</sub> is mainly promoted by the intermediate hydroxyl radicals produced via the reaction between reduced polyoxotungstate and oxygen. Those findings speak broadly to the utility of POMs to unify electrochemical and thermochemical catalysis and perhaps even photocatalysis. [20a,b]

## **Supporting Information**

The Supporting Information is available free of charge on the website.

### **Acknowledgements**

We thank the Ministry of Education of Singapore for the MOE Tier-2 grant (A-8000482-00-00, MOE-T2EP10221-0020), the National Research Foundation (NRF) of Singapore for the C4T project under CARES (WBS R-279-000-604-592), the National Natural Science Foundation of China (22178265, U21B2096, 21938008), Research Fund for International Young Scientists (22250410262), National Key Research and Development Program of (2022YFB4101702) and Tianjin Science and Technology Applied Basic Program Surface (22JCYBJC01410) for financial support.

# **Conflict of Interest**

The authors declare no conflict of interest.

#### **Data Availability Statement**

The data that support the findings of this study are available from the corresponding author upon reasonable request.

**Keywords:** Methane Partial Oxidation • Electrocatalysis • Polyoxometalates • Phosphotungstic Acid

a) H. Zhang, Z. Sun, Y. H. Hu, Renew. Sustain. Energy Rev.
 149, 111330; b) Q. Zhu, H. Zhou, L. Wang, L. Wang, C. Wang, H. Wang, W. Fang, M. He, Q. Wu, F.-S. Xiao, Nat.

- Catal. 2022, 5, 1030–1037; c) M. Akri, S. Zhao, X. Li, K. Zang, A. F. Lee, M. A. Isaacs, W. Xi, Y. Gangarajula, J. Luo, Y. Ren, Y.-T. Cui, L. Li, Y. Su, X. Pan, W. Wen, Y. Pan, K. Wilson, L. Li, B. Qiao, H. Ishii, Y.-F. Liao, A. Wang, X. Wang, T. Zhang, Nat. Commun. 2019, 10, 5181.
- [2] a) N. F. Dummer, D. J. Willock, Q. He, M. J. Howard, R. J. Lewis, G. Qi, S. H. Taylor, J. Xu, D. Bethell, C. J. Kiely, G. J. Hutchings, *Chem. Rev.* 2023, 123, 6359–6411; b) P. Schwach, X. Pan, X. Bao, *Chem. Rev.* 2017, 117, 8497–8520; c) Y. Tang, Y. Li, F. Feng Tao, *Chem. Soc. Rev.* 2022, 51, 376–423.
- [3] a) C. Hammond, M. M. Forde, M. H. Ab Rahim, A. Thetford, Q. He, R. L. Jenkins, N. Dimitratos, J. A. Lopez-Sanchez, N. F. Dummer, D. M. Murphy, A. F. Carley, S. H. Taylor, D. J. Willock, E. E. Stangland, J. Kang, H. Hagen, C. J. Kiely, G. J. Hutchings, *Angew. Chem. Int. Ed.* 2012, 51, 5129–5133; b) P. Tomkins, A. Mansouri, S. E. Bozbag, F. Krumeich, M. B. Park, E. M. C. Alayon, M. Ranocchiari, J. A. van Bokhoven, *Angew. Chem. Int. Ed.* 2016, 55, 5467–5471.
- [4] a) J. A. Labinger, Chem. Rev. 2017, 117, 8483–8496; b) N. J. Gunsalus, A. Koppaka, S. H. Park, S. M. Bischof, B. G. Hashiguchi, R. A. Periana, Chem. Rev. 2017, 117, 8521–8573;
  c) B. G. Hashiguchi, M. M. Konnick, S. M. Bischof, S. J. Gustafson, D. Devarajan, N. Gunsalus, D. H. Ess, R. a Periana, Science (80). 2014, 343, 1232–1237; d) R. S. Kim, A. Nazemi, T. R. Cundari, Y. Surendranath, ACS Catal. 2020, 10, 14782–14792; e) R. S. Kim, E. C. Wegener, M. C. Yang, M. E. O'Reilly, S. Oh, C. H. Hendon, J. T. Miller, Y. Surendranath, J. Am. Chem. Soc. 2020, 142, 20631–20639.
- a) S. J. Freakley, N. Dimitratos, D. J. Willock, S. H. Taylor, C. J. Kiely, G. J. Hutchings, Acc. Chem. Res. 2021, 54, 2614–2623; b) B. Yu, L. Cheng, S. Dai, Y. Jiang, B. Yang, H. Li, Y. Zhao, J. Xu, Y. Zhang, C. Pan, X. Cao, Y. Zhu, Y. Lou, Adv. Sci. 2023, 2302143; c) G. Fang, F. Wei, J. Lin, Y. Zhou, L. Sun, X. Shang, S. Lin, X. Wang, J. Am. Chem. Soc. 2023, 145, 13169–13180; d) X. Cui, H. Li, Y. Wang, Y. Hu, L. Hua, H. Li, X. Han, Q. Liu, F. Yang, L. He, X. Chen, Q. Li, J. Xiao, D. Deng, X. Bao, Chem 2018, 4, 1902–1910; e) W. Zhao, Y. Shi, Y. Jiang, X. Zhang, C. Long, P. An, Y. Zhu, S. Shao, Z. Yan, G. Li, Z. Tang, Angew. Chem. Int. Ed. 2021, 60, 5811–5815.
- [6] a) A. M. Joshi, W. N. Delgass, K. T. Thomson, J. Phys. Chem. C 2007, 111, 7384-7395; b) N. Agarwal, S. J. Freakley, R. U. McVicker, S. M. Althahban, N. Dimitratos, Q. He, D. J. Morgan, R. L. Jenkins, D. J. Willock, S. H. Taylor, C. J. Kiely, G. J. Hutchings, Science (80). 2017, 358, 223-227; c) J. H. Carter, R. J. Lewis, N. Demetriou, C. Williams, T. E. Davies, T. Qin, N. F. Dummer, D. J. Morgan, D. J. Willock, X. Liu, S. H. Taylor, G. J. Hutchings, Catal. Sci. Technol. 2023, 13, 5848-5858; d) W. Wang, W. Zhou, Y. Tang, W. Cao, S. R. Docherty, F. Wu, K. Cheng, Q. Zhang, C. Copéret, Y. Wang, J. Am. Chem. Soc. 2023, 145, 12928-12934; e) Z. Jin, L. Wang, E. Zuidema, K. Mondal, M. Zhang, J. Zhang, C. Wang, X. Meng, H. Yang, C. Mesters, F.-S. Xiao, Science (80). 2020, 367, 193-197; f) F. Ni, T. Richards, L. R. Smith, D. J. Morgan, T. E. Davies, R. J. Lewis, G. J. Hutchings, ACS Org. Inorg. Au 2023, 3, 177-183; g) Y. Liu, L. Wang, F.-S. Xiao, Chem. Res. Chinese Univ. 2022, 38, 671-676.
- [7] a) S. Yuan, Y. Li, J. Peng, Y. M. Questell-Santiago, K. Akkiraju, L. Giordano, D. J. Zheng, S. Bagi, Y. Román-Leshkov, Y. Shao-Horn, Adv. Energy Mater. 2020, 10, 2002154; b) J. A. Arminio-Ravelo, M. Escudero-Escribano, Curr. Opin. Green Sustain. Chem. 2021, 30, 100489.
- [8] Y. Song, Y. Zhao, G. Nan, W. Chen, Z. Guo, S. Li, Z. Tang, W. Wei, Y. Sun, Appl. Catal. B Environ. 2020, 270, 118888.
- [9] R. S. Rocha, R. M. Reis, M. R. V. Lanza, R. Bertazzoli, Electrochim. Acta 2013, 87, 606–610.





- [10] M. J. Boyd, A. A. Latimer, C. F. Dickens, A. C. Nielander, C. Hahn, J. K. Nørskov, D. C. Higgins, T. F. Jaramillo, ACS Catal. 2019, 9, 7578–7587.
- [11] J. Chang, L. Song, Y. Xu, Y. Ma, C. Liang, W. Jiang, Y. Zhang, Nano Res. 2020, 13, 67–71.
- [12] a) M. S. A. Sher Shah, C. Oh, H. Park, Y. J. Hwang, M. Ma, J. H. Park, Adv. Sci. 2020, 7, 2001946; b) M. Ma, C. Oh, J. Kim, J. H. Moon, J. H. Park, Appl. Catal. B Environ. 2019, 259, 118095; c) C. Kim, H. Min, J. Kim, J. Sul, J. Yang, J. H. Moon, Appl. Catal. B Environ. 2023, 323, 122129; d) J. Lee, S. Lee, C. Kim, J. S. Yoo, J. H. Moon, Appl. Catal. B Environ. 2024, 344, 123633; e) J. Lee, J. Yang, J. H. Moon, ACS Energy Lett. 2021, 6, 893–899; f) C. Kim, H. Min, J. Kim, J. H. Moon, Energy Environ. Sci. 2023, 16, 3158–3165; g) A. Mehmood, S. Y. Chae, E. D. Park, Catalysts 2024, 14, 58.
- [13] a) X. Meng, X. Cui, N. P. Rajan, L. Yu, D. Deng, X. Bao, Chem 2019, 5, 2296–2325; b) Q. Wang, M. Kan, Q. Han, G. Zheng, Small Struct. 2021, 2, 2100037; c) R. S. Kim, Y. Surendranath, ACS Cent. Sci. 2019, 5, 1179–1186; d) S. Xie, S. Lin, Q. Zhang, Z. Tian, Y. Wang, J. Energy Chem. 2018, 27, 1629– 1636.
- [14] a) J. Deng, S. Lin, J. T. Fuller, B. Zandkarimi, H. M. Chen, A. N. Alexandrova, C. Liu, *Angew. Chem. Int. Ed.* 2021, 60, 26630–26638; b) D. Xiang, J. A. Iñiguez, J. Deng, X. Guan, A. Martinez, C. Liu, *Angew. Chem. Int. Ed.* 2021, 60, 18152–18161; c) J. Deng, S.-C. Lin, J. Fuller, J. A. Iñiguez, D. Xiang, D. Yang, G. Chan, H. M. Chen, A. N. Alexandrova, C. Liu, *Nat. Commun.* 2020, 11, 3686.
- [15] A. M. Khenkin, A. Herman, E. Haviv, R. Neumann, ACS Catal. 2021, 11, 10494–10501.
- [16] J. Kim, J. H. Kim, C. Oh, H. Yun, E. Lee, H.-S. Oh, J. H. Park, Y. J. Hwang, *Nat. Commun.* 2023, 14, 4704.
- [17] a) C. W. Koo, A. C. Rosenzweig, *Chem. Soc. Rev.* 2021, 50, 3424–3436; b) S. Sirajuddin, A. C. Rosenzweig, *Biochemistry* 2015, 54, 2283–2294.
- [18] a) M. Bugnola, K. Shen, E. Haviv, R. Neumann, ACS Catal. 2020, 10, 4227–4237; b) M. Bugnola, R. Carmieli, R. Neumann, ACS Catal. 2018, 8, 3232–3236.
- [19] a) M. J. Hülsey, V. Fung, X. Hou, J. Wu, N. Yan, Angew. Chem. Int. Ed. 2022, 61, e202208237; b) M. J. Hülsey, S. Baskaran, S. Ding, S. Wang, H. Asakura, S. Furukawa, S. Xi, Q. Yu, C. Q. Xu, J. Li, N. Yan, CCS Chem. 2022, 4, 3296–3308; c) M. J. Hülsey, B. Zhang, Z. Ma, H. Asakura, D. A. Do, W. Chen, T. Tanaka, P. Zhang, Z. Wu, N. Yan, Nat. Commun. 2019, 10, 1330; d) K. Kamata, K. Yonehara, Y. Nakagawa, K. Uehara, N. Mizuno, Nat. Chem. 2010, 2, 478–483; e) I. A. Weinstock, R. E. Schreiber, R. Neumann, Chem. Rev. 2018, 118, 2680–2717; f) A. D. Stergiou, M. D. Symes, Catal. Today 2022, 384–386, 146–155.
- [20] a) B. An, Z. Li, Z. Wang, X. Zeng, X. Han, Y. Cheng, A. M. Sheveleva, Z. Zhang, F. Tuna, E. J. L. McInnes, M. D. Frogley, A. J. Ramirez-Cuesta, L. S. Natrajan, C. Wang, W. Lin, S. Yang, M. Schröder, Nat. Mater. 2022, 21, 932–938; b) C. Dong, M. Marinova, K. Ben Tayeb, O. V. Safonova, Y. Zhou, D. Hu, S. Chernyak, M. Corda, J. Zaffran, A. Y. Khodakov, V. V. Ordomsky, J. Am. Chem. Soc. 2023, 145, 1185–1193; c) N. Mizuno, H. Ishige, Y. Seki, M. Misono, D.-J. Suh, W. Han, T.

- Kudo, Chem. Commun. 1997, 2, 1295–1296; d) J.-S. Min, H. Ishige, M. Misono, N. Mizuno, J. Catal. 2001, 198, 116–121;
  e) I. Bar-Nahum, A. M. Khenkin, R. Neumann, J. Am. Chem. Soc. 2004, 126, 10236–10237.
- [21] S. Wang, V. Fung, M. J. Hülsey, X. Liang, Z. Yu, J. Chang, A. Folli, R. J. Lewis, G. J. Hutchings, Q. He, N. Yan, *Nat. Catal.* 2023, 6, 895–905.
- [22] J. Chang, M. J. Hülsey, S. Wang, M. Li, X. Ma, N. Yan, Angew. Chem. Int. Ed. 2023, 62, e202218265.
- [23] L. MacDonald, J. C. McGlynn, N. Irvine, I. Alshibane, L. G. Bloor, B. Rausch, J. S. J. Hargreaves, L. Cronin, Sustain. Energy Fuels 2017, 1, 1782–1787.
- [24] T. Feng, H. Wang, Y. Liu, J. Zhang, Y. Xiang, S. Lu, J. Power Sources 2019, 436, 226831.
- [25] B. Rausch, M. D. Symes, G. Chisholm, L. Cronin, *Science* (80). 2014, 345, 1326–1330.
- [26] F. Y. Xie, L. Gong, X. Liu, Y. T. Tao, W. H. Zhang, S. H. Chen, H. Meng, J. Chen, J. Electron Spectros. Relat. Phenomena 2012, 185, 112–118.
- [27] W. Zhou, J. Gao, Y. Ding, H. Zhao, X. Meng, Y. Wang, K. Kou, Y. Xu, S. Wu, Y. Qin, Chem. Eng. J. 2018, 338, 709–718.
- [28] a) Y. V. Geletii, C. L. Hill, R. H. Atalla, I. A. Weinstock, J. Am. Chem. Soc. 2006, 128, 17033–17042; b) O. Snir, Y. Wang, M. E. Tuckerman, Y. V. Geletii, I. A. Weinstock, J. Am. Chem. Soc. 2010, 132, 11678–11691.
- [29] W. Feng, T. R. Zhang, Y. Liu, R. Lu, Y. Y. Zhao, J. N. Yao, J. Mater. Sci. 2003, 38, 1045–1048.
- [30] V. Leandri, J. M. Gardner, M. Jonsson, J. Phys. Chem. C 2019, 123, 6667–6674.
- [31] L. Luo, L. Fu, H. Liu, Y. Xu, J. Xing, C.-R. Chang, D.-Y. Yang, J. Tang, *Nat. Commun.* 2022, 13, 2930.
- [32] a) E. Finkelstein, G. M. Rosen, E. J. Rauckman, J. Am. Chem. Soc. 1980, 102, 4994–4999; b) M. Kohno, E. Sato, N. Yaeka-shiwa, T. Mokudai, Y. Niwano, Chem. Lett. 2009, 38, 302–307.
- [33] Y. Jiang, Y. Fan, S. Li, Z. Tang, CCS Chem. 2023, 5, 30-54.
- [34] B. Yang, J. J. Pignatello, D. Qu, B. Xing, J. Phys. Chem. A 2015, 119, 1055–1065.
- [35] a) H. Zhang, W. Zhong, Q. Gong, P. Sun, X. Fei, X. Wu, S. Xu, Q. Zhang, G. Fu, S. Xie, Y. Wang, Angew. Chem. Int. Ed. 2023, 62, e202303405; b) Y. Fan, W. Zhou, X. Qiu, H. Li, Y. Jiang, Z. Sun, D. Han, L. Niu, Z. Tang, Nat. Sustain. 2021, 4, 509–515; c) S. Xie, W. Ma, X. Wu, H. Zhang, Q. Zhang, Y. Wang, Y. Wang, Energy Environ. Sci. 2021, 14, 37–89.
- [36] a) M. A. Ali, B. Muthiah, Catalysts 2022, 12, 133; b) B. Wang, H. Hou, Y. Gu, Chem. Phys. Lett. 1999, 309, 274–278.
- [37] W. E. Wilson, A. A. Westenberg, Symp. Combust. 1967, 11, 1143–1150.
- [38] M. H. Ab Rahim, M. M. Forde, R. L. Jenkins, C. Hammond, Q. He, N. Dimitratos, J. A. Lopez-Sanchez, A. F. Carley, S. H. Taylor, D. J. Willock, D. M. Murphy, C. J. Kiely, G. J. Hutchings, *Angew. Chem. Int. Ed.* 2013, 52, 1280–1284.

Manuscript received: September 8, 2024 Accepted manuscript online: October 26, 2024 Version of record online: November 18, 2024